PHOTONICS Research

Covert wireless communication using massive optical comb channels for deep denoising

Xianglei Yan,[1,2] Xihua Zou,[1,2,*] Peixuan Li,[1,2] Wei Pan,[1,2] and Lianshan Yan[1,2]

[1]Center for Information Photonics and Communications, School of Information Science and Technology, Southwest Jiaotong University, Chengdu 611756, China
[2]International Cooperation Research Center of China: Communications & Sensor Networks for Modern Transportation, Chengdu 611756, China
*Corresponding author: zouxihua@swjtu.edu.cn

Received 13 January 2021; revised 6 April 2021; accepted 8 April 2021; posted 13 April 2021 (Doc. ID 419605); published 28 May 2021

Covert wireless communications are unprecedentedly vital for security and privacy of individuals, government, and military bodies. Besides encryption, hiding signal transmission deeply under noise background highly proliferates the covertness in the physical layer. A deep signal hiding leads to a low interception probability at the interceptor but a poor data recovery at the receiver. To ensure both high covertness and high-fidelity recovery, massive and dense optical comb channels are utilized for deep denoising through the analog spectrum convolution. Using an external modulation-based optical frequency comb (OFC) and a single detection branch, the available optical comb channels can sustainably scale up by breaking or greatly mitigating physical bottlenecks on immense hardware and spectrum requirements. Thus, a striking signal-to-noise ratio (SNR) rise can be achieved for deep denoising. Combination of 1024 comb channels (the first parallel comb channel number beyond 1000) and the analog spectrum convolution enable a record SNR enhancement of 29 dB for a microwave signal with a 10.24 GHz bandwidth and a 10 Mbit/s data rate, which is deeply hidden below the in-band noises by 18 dB or even 30 dB in both the frequency and time domains. This method opens a new avenue for covert communications. © 2021 Chinese Laser Press

https://doi.org/10.1364/PRJ.419605

1. INTRODUCTION

Wireless communications have already penetrated into all corners of our society, with the increasing tides of 5G/B5G, internet of things, ubiquitous access, and cloud computing [1]. Accordingly, the covertness of today's wireless communications attracts unprecedented interest, when facing great risks to individual privacy and government and military security. As such, the covert wireless communication to achieve a reliable information transmission from transmitter to receiver with low probability of interception has been the focus of academic, industrial, and military communities. Traditionally, besides the encryption methods for content protection, the communication covertness can be enhanced through the electromagnetic signal protection in the physical layer [2–4]. Hiding the transmitting signal deeply under the noise or interference background is one of the prevailing methods to reinforce the physical layer security [5–7]. Furthermore, if the interceptor cannot detect the underlying signal transmission between the transmitter and the receiver, there is no opportunity to launch an "eavesdropping and decoding" attack, even with unlimited computing resource or decryption codes [7]. In general, the deeper the transmitting signal is hid under the noise background with a worse signal-to-noise ratio (SNR), the lower the interception probability for the adversary is [5]. This ensures a higher transmission covertness between transmitter and receiver. However, there is usually a trade-off between the covertness and the fidelity of signal recovery, since a deeper hiding would result in a higher bit error rate (BER) at receiver. To ensure both high covertness and high-fidelity signal recovery, deep hiding and deep denoising should be synchronously satisfied.

Fortunately, the optical frequency comb (OFC), empowering intrinsic coherent exploitation of the overall electromagnetic spectrum [8–10], is generated to have a series of discrete correlated optical comb lines (or teeth) with equal spectral spacing in microwave size [11–20]. In theory, the OFCs are capable of providing enormous comb channels for high-sensitivity spectroscopy and high-capacity microwave/optical signal processing [21–26], as well as for deep denoising in sub-noise signal recovery when facing a weak signal or a poor SNR [27–30]. For instance, dual OFCs help to multicast the signal spectrum into multiple replicas through multiple comb lines and then slice the spectrum into a series of subbands (or channels). The coherent stacking of each subband in phase leads to an SNR increase or a net gain linearly proportional to the available subband or channel number. In Ref. [28] the detection of a

fast subnoise signal with a big bandwidth and a low power level was implemented with an SNR improvement of 14.1 dB by using dual OFCs, wherein 36 comb lines were generated for signal spectrum replication and coherent stacking. In a follow-up experiment using more than 300 comb lines [29], the SNR was improved by 23.8 dB in contrast to the ideal value of 24.7 dB.

However, the comb channel scalability and the resultant superior limit of SNR increase are unsustainable because of physical bottlenecks on complicated opto-electronic hardware and immense spectrum resources to support massive optical comb channels. In the reports [28,29], dual coherent OFCs with slightly different large free spectral ranges were generated to form a few comb-line pairs, and each pair corresponds to a coherent comb channel. All comb channels are wavelength demultiplexed, and then an inter-frequency (IF) filter and an individual coherent detection are needed for each channel to implement mutual beating between two paired comb lines, requiring dramatically complicated opto-electronic hardware whose size is proportional to the channel number. In this way, it is costly and bulky to support over 100 parallel comb channels, and it is extremely challenging and even impossible with thousands of comb channels. Moreover, the available comb channel number is also constrained by the available wavelength range (i.e., limited spectrum resource). Large comb spacings or coarse comb lines are inevitable for avoiding the beat noises or interference among comb lines and signals, making massive coherent combs nearly impossible. For a large comb spacing (e.g., 0.4 nm [28]) or coarsely distributed comb lines, less than 90 channels are implemented within a given wavelength range such as the C band (e.g., 1530–1565 nm), such that the deep denoising for covert wireless communication is critically degraded.

Here an efficient covert wireless communication system is proposed and demonstrated using deep signal hiding with a very poor incident SNR and deep denoising with a striking SNR rise, wherein massive optical comb channels are enabled by breaking the physical bottlenecks on immense opto-electronic hardware and wavelength resource requirements. In the communication setup, a designed transmitting signal is deeply hidden or heavily contaminated in both the frequency and time domains, for the purpose of high covertness or low interception probability. Massive spectral slices are replicated and then coherently stacked in phase through the analog spectrum convolution. This unique convolution outperforms the digital spectrum convolution or waveform cross-correlation operation in spread spectrum communication in terms of being ultrafast, having nearly zero latency, and having memoryless analog operation. As such, the signal's power level is greatly proliferated in a coherent mode, but the noise level retains nearly unchanged in an incoherent mode. Thus, the deep denoising is achieved for subnoise signal recovery with a striking SNR improvement. As a demonstration, an OFC with 1024 comb lines and a 10 MHz comb spacing is generated for detecting and recovering an incident microwave signal with a 10.24 GHz bandwidth, a 10 Mbit/s data rate, and a poor SNR ranging from −30 to −18 dB for deep signal hiding. After the deep coherent denoising, an SNR improvement of 29 dB is experimentally achieved, in high line with the theoretical value of 30 dB. It should be highlighted that the coherent comb channels and the SNR can be further multiplied in proportion to the channel number by involving more comb lines. Here the saturated input/output power of the balanced photodetector (BPD) will set a slight limitation on the further increase of the recovered signal's power when the comb line number is already big enough.

2. COVERT WIRELESS COMMUNICATION SYSTEM USING MASSIVE COMB CHANNELS

The covert communication system using massive comb channels is depicted in Fig. 1, consisting of a transmitting unit for deep hiding and a receiving unit for deep denoising. The original data is processed to have weak, flat spectral and temporal envelopes in the microwave domain, which is deeply hidden below noise in both the frequency and time domains. Such

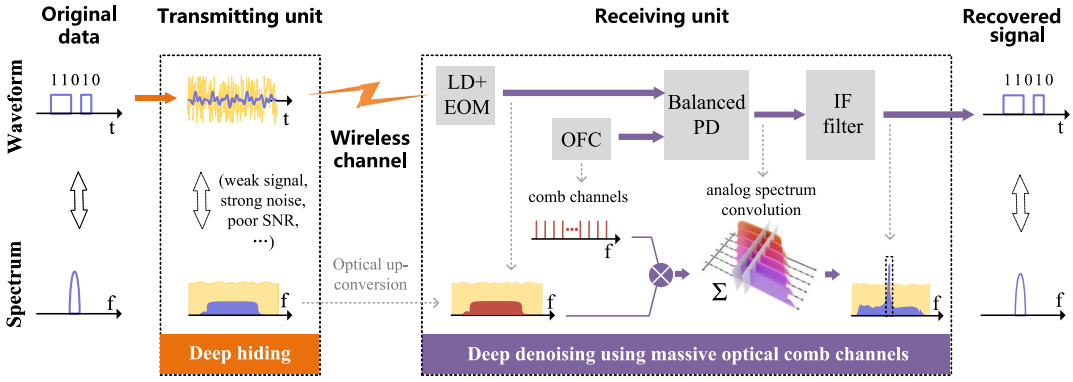

Fig. 1. Schematic diagram of the covert wireless communication system using massive comb channels. In the transmitting unit the microwave signal is designed to have a flat and large bandwidth and is deeply hidden by strong in-band noises in both the frequency and time domains. In the receiving unit, the transmitting microwave signal is received to modulate an optical carrier, forming an incident microwave photonic signal. A flat OFC is generated with massive and ultradense comb lines for implementing analog spectrum convolution between the OFC and the incident microwave photonic signal, leading to massive spectral replication of the transmitting signal and then a coherent in-phase stacking of massive spectral replicas at the IF point. Extracting the IF signal through a bandpass filter enables the deep denoising for signal recovery, showing a huge SNR improvement. (EOM, electro-optic modulator; IF, inter-frequency; LD, laser diode; OFC, optical frequency comb; PD, photodetector.)

a noisy microwave signal with a weak power level and a poor SNR is radiated toward the receiving unit through the wireless channel. In the receiving unit, the acquired microwave signal is modulated on an optical carrier through electro-optic modulation, generating the incident microwave photonic signal. Actually, the incident microwave photonic signal is identical or equivalent to the transmitting microwave signal, except for the central frequency being up-converted from the microwave to the optical domain in single sideband modulation mode. Next, a flat ultradense OFC with N comb lines is generated and converged with the microwave photonic signal in a BPD. An analog spectrum convolution between the OFC and the microwave photonic signal is performed, such that massive spectral replicas are formed. Each spectral replica is formed by an individual comb line, defined as a comb channel or subband corresponding to that comb line. By carefully matching the phases of the massive comb lines according to that of the transmitting signal, a coherent in-phase stacking of the massive spectral replicas is achieved in a specifically designed IF band, while avoiding signal-to-signal beating (see details in Section 4). Meanwhile, no in-phase stacking will happen for noise due to its random and incoherent phase [30].

Therefore, a huge SNR improvement proportional to the comb channel number can be achieved at the IF point. The received transmitting microwave signal or the incident microwave photonic signal can be deeply denoised, and the original data can be correctly recovered through the IF signal. In this way, both high covertness and high-fidelity signal recovery are ensured in this OFC-enabled wireless communication system.

A. Deep Hiding with Poor SNR in Both the Frequency and Time Domains

For high covertness, deep signal hiding is implemented in the transmitting unit. White Gaussian noises or other artificial noises and interferences [6] with a relatively higher power level are generated to deeply bury the microwave signal before radiation out. Along the flat and broadband weak power distribution of the microwave signal, the in-band SNR in the frequency domain should be as low as −20 or −30 dB. However, only a poor SNR in the frequency domain is not sufficient to ensure a low interception probability, since the high or faint peaks in the time domain will still reveal the covertness. For such, a nearly uniform envelope in the time domain is ensured by applying a random phase distribution among the overall bandwidth of the transmitting microwave signal, instead of a pulsed or concentrated one in classic ultra-wideband communication systems. Details are introduced in the Section 2.D. As a result, deep hiding is achieved in both the frequency and time domains for the transmitting microwave signal.

B. Photonic Assisted Analog Spectrum Convolution

The key to the success of the covert communication lies in the deep denoising at the receiving unit, which is implemented by using analog spectrum convolution and massive coherent stacking. Mathematically, we start from a flat and ultradense OFC with N comb lines, derived as

$$C(\omega) = \sum_{n=0}^{N-1} A_n \exp(j\phi_n)\delta(\omega - \omega_c - n\Delta\omega_c), \tag{1}$$

where $\delta(\cdot)$ is the Dirac function, A_n and ϕ_n are the amplitude and the phase of the nth comb line for $n \in [0, N-1]$, and ω_c and $\Delta\omega_c$ represent the starting frequency and the comb spacing, respectively. Accordingly, a spectral range (i.e., bandwidth) close to $N\Delta\omega_c$ can be covered. Correspondingly, $c(t)$ is defined as the temporal waveform of the OFC.

The incident microwave photonic signal covers a frequency range from ω_s to $\omega_s + B_s$, expressed as

$$S(\omega) = \begin{cases} A_s(\omega)\exp j\phi_s(\omega), & \text{if } \omega_s \le \omega \le \omega_s + B_s, \\ \text{else}, & \text{else}, \end{cases} \tag{2}$$

where $A_s(\omega)$ and $\phi_s(\omega)$ are the amplitude and the phase at the angular frequency of ω, ω_s is the starting frequency, B_s is the bandwidth, and "else" means other spectral components with lower powers. Also, its temporal waveform is defined as $s(t)$.

When the OFC and the incident microwave photonic signal are coupled into the BPD, an output signal is derived as

$$y(t) \propto |c(t) + s(t)|^2 - |c(t) - s(t)|^2 = 2c(t)\cdot s^*(t) + \text{c.c.}, \tag{3}$$

where $|\cdot|$ represents the absolute value operator and c.c. represents the conjugated component. The term $c(t)\cdot s^*(t)$ in Eq. (3) can be written in its frequency version as

$$Y_1(\omega) = \frac{1}{2\pi} C(\omega) \otimes S^*(-\omega), \tag{4}$$

where $\otimes$ represents the convolution operator. Actually, $C(\omega)$ and $S(\omega)$ are the Fourier transforms of the two temporal waveforms of $c(t)$ and $s(t)$, respectively.

Here $\omega_c \ge \omega_s$ is assumed for deriving a simple expression, as the IF point is only determined by the relative frequency difference between $c(t)$ and $s(t)$. Also, $\Delta B = B_s - N\Delta\omega_c$, defined as the bandwidth difference between $s(t)$ and $c(t)$, is set to be nonnegative to ensure an available IF bandwidth for effectively stacking massive replicated spectral slices. In this case, all the N replicated spectra are located in their desired spectral slices within a specific frequency range of $\omega_c - \omega_s - \Delta B \le \omega \le \omega_c - \omega_s$. Within this specific frequency range, Eq. (4) can be rewritten as

$$Y_1(\omega) = \frac{1}{2\pi}\sum_{n=0}^{N-1} A_n \exp(j\phi_n) S^*(\omega_c + n\Delta\omega_c - \omega). \tag{5}$$

Equation (5) shows the analog spectrum convolution of the OFC and the photonic signal, which is equivalently described in the electrical domain through opto-electrical conversion using the BPD. The analog spectrum convolution, showing ultrafast and memoryless advantages over digital convolution or correlation operations in, for example, traditional spread spectrum communications, can be regarded as the sum of multiple weighted (both amplitude and phase) replicas of inversed and frequency-shifted spectrum of the photonic signal.

For a vivid demonstration of analog spectrum convolution, Fig. 2 shows the detailed process happening in the BPD. As depicted in Fig. 2(a), the spectrum of the incident microwave photonic signal is massively replicated, and the IF point locates in the overlapping range of all replicated spectra. Through the in-phase coherent stacking, the recovered signal at the IF point has a high amplitude gain as illustrated in Fig. 2(b). Meanwhile, as a comparison, the in-phase coherent stacking for the incident

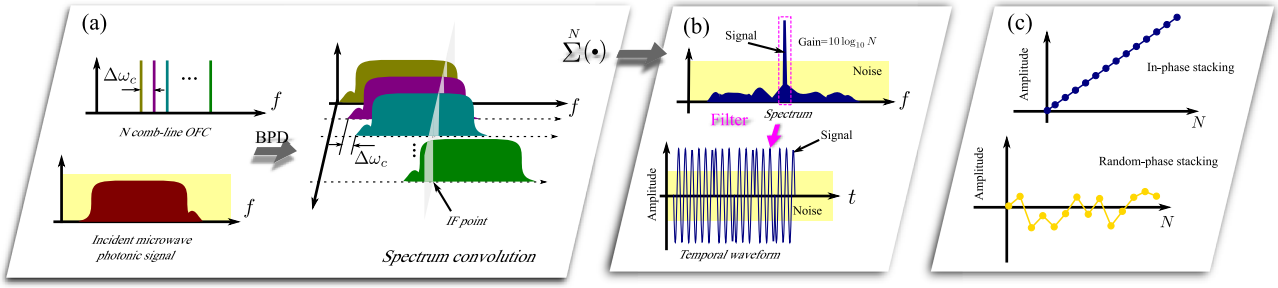

Fig. 2. (a) Analog spectrum convolution in BPD. (b) Recovered signal at the IF point. (c) Comparison between in-phase coherent stacking and random-phase incoherent stacking.

microwave photonic signal and random-phase incoherent stacking for the white Gaussian noise are shown Fig. 2(c). Obviously, the incident microwave photonic signal will get an amplitude (or power) gain from the in-phase stacking, while no amplitude (or power) gain for the noise. Such a principle is just behind the SNR improvement of our covert communication system, which will be explained with more detail in the following.

C. SNR Improvement for Deep Denoising

To quantitatively analyze the SNR improvement from the deep denoising, both the OFC and the incident microwave photonic signal (equivalently the transmitting microwave signal) are designed to have relative flat spectral envelopes. Furthermore, A_n and $A_s(\omega)$ can be simplified as constant values, A_0 and A_s. In this case, the performance of coherent stacking will only be determined by two phase terms ϕ_n and ϕ_s. On the one hand, when the two phase terms are randomly distributed without mutual correlation between them, the summation or the coherent stacking [see Eq. (5)] will lead to a mass spectrum. On the other hand, when the two phase terms are correlated with a constant difference (e.g., zero for the simplest case), an in-phase coherent stacking can be achieved for SNR enhancement. In this covert communication system, a constant phase difference is adopted and pre-implemented during the deep hiding procedure at the transmitting unit.

For SNR analysis, we have to first extract the IF signal at the IF point defined as $\omega_m = \omega_c - \omega_s - (1-\varepsilon)\Delta B$, where $\varepsilon \in [0,1]$ is a coefficient. Here the phase relationship between the OFC and the microwave photonic signal can be optimized as $\phi_n = \phi_s[\omega_s + (1-\varepsilon)\Delta B + n\Delta\omega_c]$, and a non-constant or random phase function is desirable for the OFC (see the following Section 2.D). As a result, at the IF band Eqs. (5) and (3) can be simplified as Eqs. (6) and (7), respectively. It is clear that a huge gain linearly proportional to the number of comb lines (i.e., comb channel number) provided by the OFC can be achieved at the IF point. In the meantime, at other frequency points such an in-phase stacking will not occur among the replicated spectra, showing nearly zero mean value arising from massive random stacking and cross-cancellation. The same phenomenon will happen for noise stacking (e.g., white Gaussian noise), since the phases of noise are also randomly distributed.

$$Y_1(\omega_m) = N\frac{A_0 A_s}{2\pi}, \tag{6}$$

$$y_{\omega_m}(t) = N\frac{2A_0 A_s}{\pi}\cos(\omega_m t). \tag{7}$$

It is clear that a huge gain linearly proportional to the number of comb lines (i.e., comb channel number N) provided by the OFC can be achieved at the IF point, and the output average power can be derived as

$$P_{\omega_m}(N) = \frac{1}{2}\left(N\frac{2A_0 A_s}{\pi}\right)^2. \tag{8}$$

For the noise (e.g., white Gaussian noise), an in-phase stacking will not occur since its phase is randomly distributed. Let us define the original average spectral power of the white Gaussian noise along with the incident microwave photonic signal is n_0^2. According to its constant power spectral density, the average power at the IF point after the stacking described in Eq. (5) is increased to

$$n^2(N) = N\left(\frac{2A_0 n_0}{\pi}\right)^2, \tag{9}$$

where $(2A_0)/\pi$ indicates the growth of the amplitude gain and N comes from the sum of the power when stacking. Therefore, the SNR can be derived as

$$\mathrm{SNR}(N) = P_{\omega_m}(N)/n^2(N) = \frac{1}{2}N\left(\frac{A_s}{n_0}\right)^2. \tag{10}$$

Equation (10) reveals a linear SNR rise along with the comb line number. Being compared with a conventional method wherein the OFC is replaced by one comb line (or one optical carrier) having the same amplitude of A_0, the quantitative SNR improvement is logarithmically derived in decibels (dB) as

$$G_{\mathrm{SNR}} = 10\log_{10}[\mathrm{SNR}(N)/\mathrm{SNR}(1)] = 10\log_{10}N. \tag{11}$$

This distinct feature empowers the deep signal denoising and the high-fidelity signal recovery with a striking SNR rise through analog spectrum convolution and in-phase coherent stacking of massive replicated comb channels.

D. Random Phases for Transmitting Microwave Signal and Massive Optical Comb Lines

To reinforce the low interception probability, either the transmitting microwave signal or the OFC should not be specified to have constant phase distribution within the effective bandwidth, to avoid a high peak in the time domain.

Besides a wide bandwidth and a low, flat spectral envelope, which enable the coherent in-phase stacking of massive spectral slices, the incident microwave signal is also required to have random phase distribution. Given a constant phase distribution, a high peak will appear and make the transmitting microwave signal easily detected in the time domain, which disables the low-interception feature regardless of a poor SNR or a weak average power level. Therefore, a random (actually pseudorandom) phase distribution is designed to provide a relatively uniform, weak power distribution in the time domain for high covertness. The peak to average power ratio (PAPR) of a 10.24 GHz wideband signal can be reduced by more than 200 times when using a randomly distributed phase instead of a constant one in our experiment. Besides, the random phase distribution can be reused for a long time, with very low risk on communication vulnerability, due to the deep hiding in the physical layer and extreme complexity for brute force attacks. Moreover, for a dynamically changed random phase distribution to improve the covertness further, the overhead for transmitting of the random phase key is still very small.

The same situation applies for the phase distribution of the OFC used. An OFC is usually with constant or weak-perturbation phase distribution among comb lines, which dominantly determines its temporal waveform such as soliton pulses or other pulses [11–16,18,19]. If such a constant or weak-perturbation phase distribution is implemented, several negative problems obviously occur by considering the extremely nonuniform temporal power distribution and the high peak power. First, the high peak impedes their subsequent amplification in the fiber link. Second, the high peak will bring nonlinear distortions [31] and even equipment damage [32,33]. Therefore, a random or pseudorandom phase is optimized and applied to make a relative uniform power distribution in the time domain for the OFC. More importantly, the random phase distribution of the transmitting microwave signal should synchronously match the OFC's random phase distribution to achieve massive in-phase spectrum stacking for deep denoising.

In addition, the unbalance of the BPD will introduce some signal-to-signal beating notes or noises in the low frequency range, arising from the self-beating of the incident microwave photonic signal and the OFC. Fortunately, by using a random phase distribution, different beat notes at the same frequency are generated with random phases, and then the coherent stackings among them will randomly cancel each other. This phenomenon has twofold benefits: avoiding the signal-to-signal beat noises to signal recovery and relaxing the saturated output power of the BPD.

E. Breaking Physical Bottlenecks on Immense Hardware and Spectrum Resource Requirements

Traditional coherent denoising methods replicate the target microwave signal in parallel paths and then coherently stack them to improve the SNR [27]. However, immense requirements on hardware and spectrum resources set critical physical bottlenecks for massive comb channels, when facing a huge SNR improvement requirement from deep denoising after deep hiding. The physical bottlenecks are understood in two aspects. First, each comb-line pair with two comb lines from dual combs should be wavelength demultiplexed and then detected parallelly and separately in individual mode [28,29] to form one comb channel. Massive comb channels will require a dramatically complicated opto-electronic hardware consisting of parallel demultiplexing and detection branches proportional to the comb channel number. Such a hardware complexity is unsustainable, costly, and bulky for supporting thousands of channels and more. Second, when all comb-line pairs (comb channels) are detected in one joint branch without wavelength demultiplexing and individual detection, large comb spacings or sparse comb lines should be specified to avoid the harmful self-beating noises among different comb lines and the incident microwave photonic signal. Massive comb channels will request a dramatically wide optical spectrum proportional to the comb channel number, due to the low spectral efficiency. Such a wide spectrum is also extremely challenging and even impossible for accommodating thousands of channels and more. As an example, 1000 channels with a comb spacing of 0.4 nm will occupy a 400 nm spectrum resource, which is far beyond the total bandwidth of low-loss windows (C band, L band, and U band) of optical fiber.

Fortunately, the physical bottlenecks on hardware and spectrum resources have been broken or greatly mitigated in this proposed deep denoising method, because massive comb channels are implemented using a single detection branch and a narrow wavelength bandwidth of several nanometers, while removing the linear increase on hardware complexity and the self-beat interferences. Since only one detection branch is used, the detected signal should be shifted to an IF band to eliminate the overlapped beat interference (see Section 4 for more details), requiring a higher frequency for the narrow-bandwidth IF processing in contrast to Refs. [28,29].

3. EXPERIMENTS AND DEMONSTRATIONS

A. Deep Denoising for Covert Wireless Communication

An experimental setup to implement covert wireless communication is established, using massive comb channels for deep coherent denoising through a single detection branch. As shown in Fig. 3, the original data (e.g., 11010) from a host computer is up-converted to generate a microwave signal in differential binary phase-shift keying (DBPSK) format. In the transmitting unit, the original data [i.e., a pseudorandom binary sequence (PRBS) with a 320 bit length and a 10 Mbit/s rate] is first encoded to obtain differential code which is then applied to phase modulate a microwave carrier, generating the transmitting microwave signal spanning from 1.8 to 12.04 GHz. The microwave carrier, which has a flat spectrum envelope and a random phase distribution, is designed through inverse fast Fourier transform (IFFT). Since a random phase distribution is applied, this generated transmitting microwave signal is deeply hidden below strong noise background and then radiated out.

Inside the receiving unit, the subnoise microwave signal is captured. An optical carrier from a continuous-wave and narrow-linewidth laser is split into two parts. One part is modulated by the acquired noisy microwave signal inside a Mach–Zehnder modulator (MZM) to form the incident microwave

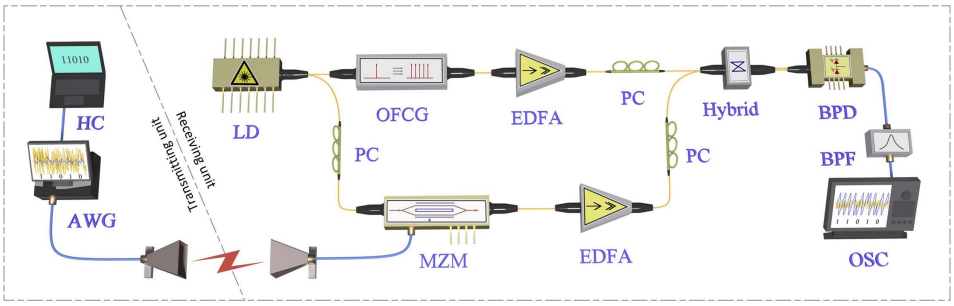

Fig. 3. Experimental setup for covert wireless communication with deep denoising method. Here the OFCG consists of a PC, an MZM, an EDFA, and an OBPF. (AWG, arbitrary waveform generator; BPD, balanced photodetector; BPF, bandpass filter at the IF point; EDFA, erbium-doped fiber amplifier; HC, host computer; Hybrid, 90° optical hybrid; LD, laser diode; MZM, Mach–Zehnder modulator; OFCG, optical frequency comb generation module; OSC; real-time oscilloscope; PC, polarization controller; OBPF, optical bandpass filter.)

photonic signal, while the other being processed to generate a customized OFC with massive and ultradense comb lines. Next, both the incident microwave photonic signal and the OFC are converged by a 90° optical hybrid and fed into a BPD simultaneously, wherein massive spectral replication and in-phase coherent stacking of massive spectral slices at the IF point are implemented. Following the BPD, an electrical bandpass filter with twice the bandwidth of the original data is employed to extract the spectral components falling inside the IF band. Then the differential coherent demodulation is implemented to recover the original data carried by the transmitting microwave signal with a much higher SNR. Consequently, the original data is recovered from strong noise background and then recorded by using a real-time oscilloscope.

As aforementioned, a random phase distribution is designed for the transmitting microwave signal to keep a low, uniform power distribution in both the frequency and time domains. Figure 4(a) shows the normalized temporal waveform and the amplitude/phase spectra of the designed transmitting microwave signal having a 10.24 GHz bandwidth and a 1.8 GHz starting frequency. To quantitatively evaluate the performance of the deep denoising, PRBS data are curved on the transmitting microwave signal in DBPSK format, while white noise is added to emulate different SNRs during the deep hiding in tests. It is highlighted that here the in-band noise or SNR is considered, rather global all-band ones, since most out-band noises can be reasonably eliminated by using a matching filter. In details, Fig. 4(b) shows the temporal waveforms and spectra of the normalized transmitting microwave signal, together with white noises. Regarding an in-band SNR of −9 or −18 dB, the microwave signal is deeply buried by the noises in both the frequency and time domains. The transmitting microwave signal embedded in strong noises is applied to modulate the optical carrier inside the MZM shown in Fig. 3, generating the incident microwave photonic signal. Here the carrier-suppression modulation is carried out to alleviate the high power saturation effect inside the BPD.

Here the OFC is generated through the module depicted in Fig. 3, using a carrier-suppressed and single-sideband (CS-SSB) modulation architecture. During the OFC generation, both electrical and optical procedures are implemented. A user-defined electrical signal with a flat spectral envelope starting

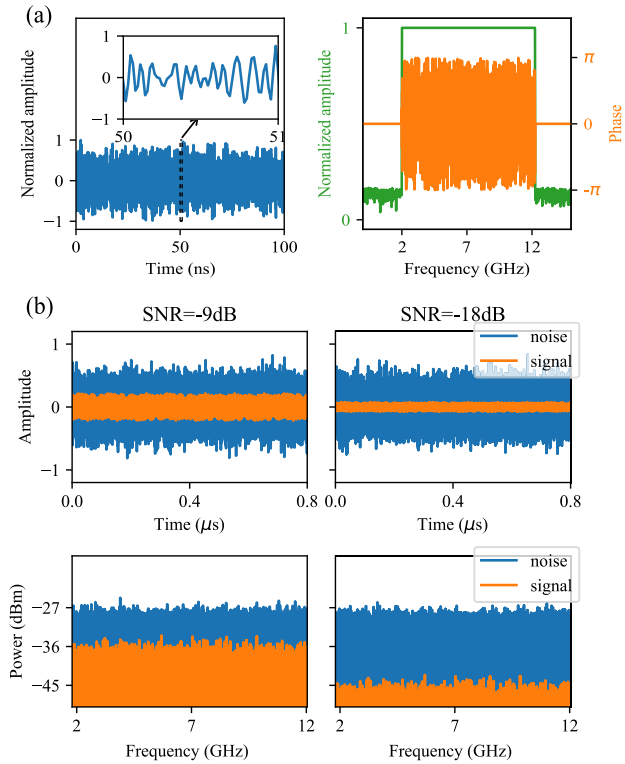

Fig. 4. Designed transmitting microwave signal and strong in-band noises during the deep hiding procedure. (a) Normalized temporal waveform (blue) and normalized spectra (amplitude spectrum, green; phase spectrum, orange) of the transmitting microwave signal. It is designed to have flat spectral and temporal envelopes, a 10.24 GHz bandwidth, and a 1.8 GHz starting frequency. (b) Illustration of the temporal waveforms and the spectra of the transmitting signals and the strong white noises, under in-band SNR of −9 or −18 dB. It is obvious that the microwave signal is deeply buried by the strong noises in both the frequency and time domains.

from 7 GHz and a random phase (corresponding to the random phase of the microwave carrier used to generate the incident microwave signal as depicted in Section 2.C) is generated from an arbitrary waveform generator (AWG, Keysight-M8195A). The user-defined electrical signal is then applied to intensity

modulate the optical carrier inside an MZM biased at the minimum point of its transfer function for carrier suppression. The generated optical signal has a flat spectral envelope starting from $f_0 + 7$ GHz (i.e., ω_c), 1024 comb lines, and a 10 MHz comb spacing, where f_0 is the frequency of the seed laser. Then a tunable optical bandpass filter is used to remove the lower sideband, while retaining the upper sideband serving as the required OFC used in communication experiments. The 7 GHz offset [see Fig. 5(a)] is set to match the optical bandpass filter.

This OFC is converged with the microwave photonic signal and the hybrid optical spectrum is also recorded. At the output of the BPD, the recovered signal after analog spectrum convolution and massive in-phase stacking is recorded and shown in Fig. 5(b), indicating a high peak power and a high SNR at the 5.2 GHz IF point (ω_m). It should be noted that a higher power only appears around the IF point, but very low powers appear for other bands of the microwave spectrum from 0 to 28 GHz due to the massive random stacking and cross-cancellation.

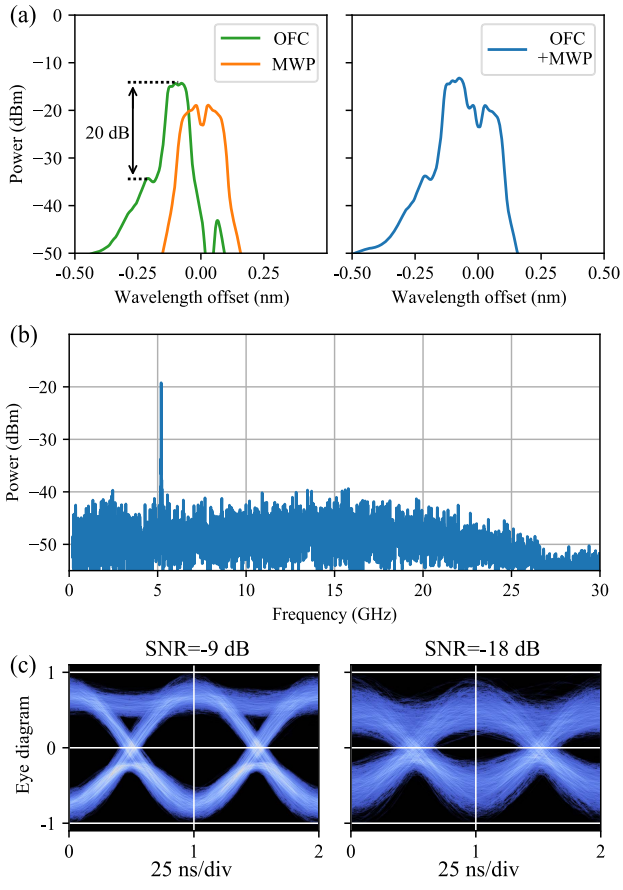

Fig. 5. Recovered signals from the experiment for covert wireless communication demonstration. (a) Optical spectra of the OFC, the incident microwave photonic signal, and the hybrid signal measured at the input of the BPD. (b) Microwave spectrum of the recovered signal observed at the output of the BPD, showing a high peak power or SNR at the 5.2 GHz IF point. (c) Eye diagrams of the recovered PRBS data from the transmitting microwave photonic signal with an SNR of −9 or −18 dB. (MWP, incident microwave photonic signal; OFC, optical frequency comb.)

In the time domain, clear and wide-open eye diagrams are achieved for PRBS data carried by the recovered signal after deep denoising as shown in Fig. 5(c). Consequently, the original data can be detected and recovered from a poor in-band SNR as low as −18 dB. Furthermore, a supplementary movie (Visualization 1) provides a vivid demonstration for this covert communication system.

B. SNR Enhancement and Performance Comparison

To quantitatively analyze the SNR enhancement of the deep denoising in the covert communication system, incident microwave photonic signals (equivalently the noisy transmitting microwave signal) with different in-band SNRs ranging from −30 to −18 dB are generated for tests. Figure 6(a) shows the BER curves measured at the covert communication experiments and a reference experiment for the purpose of performance comparision. The reference experiment is performed using the same configurations and transmitting microwave signal, but replacing the OFC with a single optical comb line or continuous-wave optical carrier.

For a given BER at 10^{-4}, an SNR improvement of 29 dB has been achieved using the deep denoising method, as compared with results of the reference experiment. Here the employment of 1024 comb lines is expected to achieve an ideal SNR improvement of 30 dB according to Eq. (11). The 1 dB gain cost in experiments mainly results from the uneven spectral

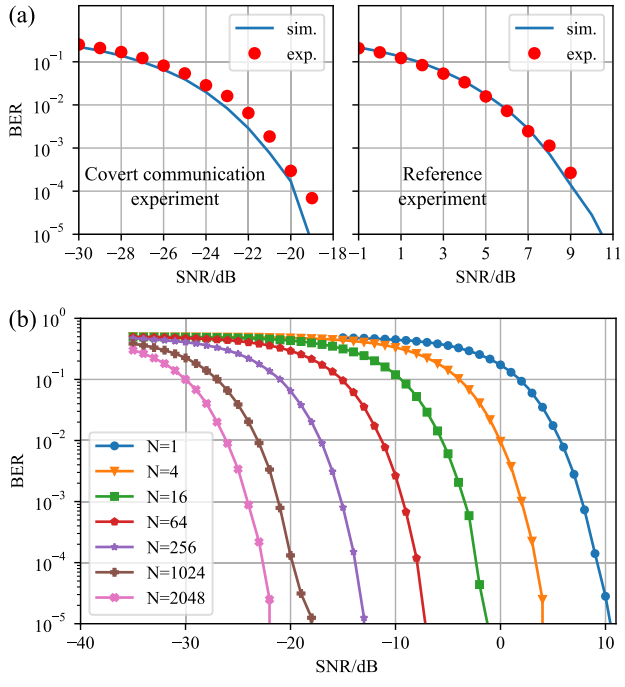

Fig. 6. BER curves measured from experiments and simulations. (a) Experimental results (red spots) and simulation results (blue solid lines) measured through the covert communication experiment (left) and the reference experiment (right). Here a single OFC with 1024 comb lines is employed, indicating a 29 dB SNR improvement at BER of 10^{-4}. (b) Simulation results measured under different comb lines ranging from 1 to 2048, indicating an SNR improvement close to the theoretical prediction of Eq. (11), being compared with one comb channel case. (BER, bit error rate; N, number of comb lines or channels.)

envelope of both the OFC and the incident microwave photonic signal, as well as nonideal configurations and parameters of the setups, such as an unstable bias voltage of the MZM or residual optical carrier of the CS-SSB modulation. In addition, a not well aligned local beam will result in a poor SNR of the received signal and reduce the SNR gain of the whole system.

To reveal the comb channel scalability or the impact of the comb channel number, simulations are carried out by gradually increasing the comb channels from 1 to 2048. The resulted BER curves for the recovered signal from the same transmitting microwave signal having a 10.24 GHz bandwidth and a 10 Mbit/s data rate are analyzed and shown in Fig. 6(b), indicating an SNR improvement well in line with Eq. (11). Consequently, the gain or the SNR rise is sustainable by using simple but elegant opto-electronic hardware.

The starting frequencies of the OFC and the incident microwave photonic signal should be carefully allocated to avoid some serious beat notes or noises, and details can be found in Section 4. In the experiments and simulations above, the OFC is generated to have a starting frequency at f_0+7 GHz (ω_c) and a bandwidth of 10.24 GHz, while the incident microwave photonic signal has a starting frequency of f_0+1.8 GHz (ω_s) and an identical bandwidth of 10.24 GHz, where f_0 is the optical carrier frequency. According to Eq. (14), the minimum difference between the two starting frequencies of the OFC and the incident microwave photonic signal is derived as 5.12 GHz when $\Delta B = 0$. Hence, the measured IF point is specified as 5.2 GHz for ensuring a beat interference-free signal recovery because a spectral overlapping ranging from 0 to 5.04 GHz will not bring any harmful interference to the IF point at 5.2 GHz.

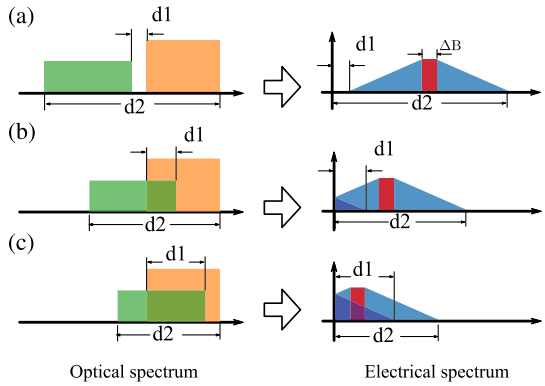

Fig. 7. Illustration of three typical situations suffering with beat noises and the optimization analysis for the starting frequencies of the OFC and the incident microwave photonic signal. The left column shows the relative positions in the frequency domain between the OFC and the incident microwave photonic signal before injecting into the BPD; the right one illustrates the corresponding spectrum positions of the recovered signal in the microwave domain. (a) No spectrum overlapping between the optical spectra of the OFC (orange block) and the incident microwave photonic signal (green block). No overlapped beat interference will happen. (b) Slight spectrum overlapping. The overlapped beat interference will happen but will not affect the IF band. (c) Heavy spectrum overlapping. The resultant interference will seriously affect the IF band and thus contaminate the deep denoising. (d_1, the difference between the microwave photonic signal's ending frequency and the OFC's starting frequency, indicating the degree of spectrum overlapping; d_2, the difference between the microwave photonic signal's starting frequency and the OFC's ending frequency, indicating the largest beat frequency; ΔB, the bandwidth difference between the microwave photonic signal and the OFC.)

4. DISCUSSION

The starting frequencies of the OFC and the incident microwave photonic signal should be carefully specified to avoid serious signal-to-signal beat notes or noises. Typically, there are three situations suffering from beat noises as shown in Fig. 7.

For simplicity, the starting frequency of the OFC (orange block) is larger than that of the incident microwave photonic signal (green block), and the bandwidth (width of orange block) of the OFC is less than that of the incident microwave photonic signal (width of green block). The subfigures on left column describe the relative position in the frequency domain before injecting into the BPD, and the ones on right column illustrate the spectrum position of the recovered microwave signal. As depicted in Fig. 7(a), when there is no overlapping between the optical spectra of the OFC and the incident microwave photonic signal, the recovered signal has a starting frequency equal to d_1 and an ending frequency equal to d_2, where d_1 and d_2 are defined in the caption of Fig. 7. Here ΔB is the bandwidth of the IF band (red range) for selecting the IF point, equal to the bandwidth difference between the incident microwave photonic signal and the OFC. When the incident microwave photonic signal and the OFC partially overlap in their spectra, as depicted in Fig. 7(b), the beat notes inside the overlapping range will contribute negative frequency components, which will in turn transform into the reflected positive ones in electrical domain and then overlap with the ordinary positive beat notes. But the reflected positive beat notes exert no harmful impact to the deep denoising as it is still away from the measured IF band. When the spectrum overlapping range between the incident microwave photonic signal and the OFC increases further [see Fig. 7(c)], the reflected positive beat notes will seriously influence the measured IF band (red range), such that the SNR enhancement will deteriorate dramatically.

To avoid beat notes arising from the third situation [Fig. 7(c)], a sufficient constraint relationship between the starting frequencies and bandwidths is derived and demonstrated in the following. The difference between their starting frequencies has a minimum value to ensure an effective IF point for beat interference-free measurement, when the bandwidth of the OFC and the incident microwave photonic signal is fixed. That means the maximum of the overlapped microwave frequency range must be smaller than the IF point inside the optional range depicted as the red block in Fig. 7. Mathematically, the constraint relationship is derived as

$$\omega_m > d_1, \tag{12}$$

where $\omega_m = \omega_c - \omega_s - (1-\varepsilon)\Delta B$ is the defined IF point. According to Figs. 7(b) and 7(c), the maximum of the overlapped microwave frequency range can be derived as

$$d_1 = \omega_s + \mathrm{B}_s - \omega_c. \tag{13}$$

By substituting Eq. (13) and the defined IF point into Eq. (12), the constraint relationship can be rewritten as

$$\omega_c - \omega_s > \frac{B_s + (1-\varepsilon)\Delta B}{2}. \quad (14)$$

From Eq. (14), the difference between their starting frequencies has a minimum value to ensure an effective IF point for beat interference-free measurement, when the bandwidth of the OFC and the incident microwave photonic signal is fixed.

Meanwhile, substituting ω_m into Eq. (14), the IF point also has a minimum value described as

$$\omega_m > \frac{B_s - (1-\varepsilon)\Delta B}{2}. \quad (15)$$

In the covert communication experiments, when facing a large-bandwidth incident microwave photonic signal, a high frequency of the IF point can be reduced by using postprocessing such as coherent detection or envelope detection.

The arrival time of the incident microwave photonic signal plays an important role in the deep denoising. A relative time delay τ between the OFC and the incident microwave photonic signal will lead to a frequency-dependent phase shift [i.e., $\exp(j\omega\tau)$], which will destroy the in-phase conditions for massive coherent stacking. On the one hand, this negative impact has been overcome here, as the arrival time of the incident microwave photonic signal can be precisely calibrated and synchronized for a cooperative communication with pilot/prior signaling. Also, slight time delay jitters arising from vibrations or temperature fluctuations can be tolerant in the experiment setup. On the other hand, this unknown time delay will enhance the covertness with a new degree of freedom against hostile interception. Due to the dense feature, the number of comb channels can be further increased to provide a higher SNR gain. But the saturated input/output power of the BPD will set a limit on the further increase of the recovered signal's power when the comb line number is already big enough.

5. CONCLUSION

A covert wireless communication system using massive comb channels has been proposed and experimentally demonstrated. Through the deep signal hiding below the noise background and the deep signal denoising from poor SNR conditions, both high covertness and high-fidelity signal recovery are realized. This simple and elegant optical system enables an ultrafast and memoryless analog spectrum convolution without complicated digital processing and breaks the physical bottlenecks on the costly and bulk opto-electronic hardware and limited optical wavelength spectrum resource for implementing massive coherent channels. In the demonstrated system, a single OFC is generated through CS-SSB modulation. The generated OFC with 1024 comb lines and an ultradense comb spacing is used for massive spectral replication and coherent in-phase stacking of massive comb channels. After deep hiding with a poor in-band SNR of −30 to −18 dB at the transmitting unit, an SNR improvement of 29 dB is achieved for recovering the microwave signal through deep denoising at the receiving unit, which can be improved further. An SNR increase proportional to the number of comb lines is ensured with excellent channel scalability. This OFC-enabled optical method paves a new and viable way for low-interception communication and weak signal detection in harsh scenarios.

Funding. National Key Research and Development Program of China (2019YFB2203200); National Natural Science Foundation of China (61922069, 61775185).

Disclosures. The authors declare no conflicts of interest.

Data Availability. Data underlying the results presented in this paper are not publicly available at this time but may be obtained from the authors upon reasonable request.

REFERENCES

1. A. Goldsmith, *Wireless Communications* (Cambridge University, 2005).
2. S. Yan, X. Zhou, J. Hu, and S. V. Hanly, "Low probability of detection communication: opportunities and challenges," IEEE Wireless Commun. **26**, 19–25 (2019).
3. Z. Liu, J. Liu, Y. Zeng, and J. Ma, "Covert wireless communication in IOT network: from AWGN channel to THz band," IEEE Internet Things **7**, 3378–3388 (2020).
4. M. K. Simon, J. K. Omura, R. A. Scholtz, and B. K. Levitt, *Spread Spectrum Communications Handbook* (Citeseer, 1994).
5. B. A. Bash, D. Goeckel, D. Towsley, and S. Guha, "Hiding information in noise: fundamental limits of covert wireless communication," IEEE Commun. Mag. **53**, 26–31 (2015).
6. R. Soltani, D. Goeckel, D. Towsley, B. A. Bash, and S. Guha, "Covert wireless communication with artificial noise generation," IEEE Trans. Wireless Commun. **17**, 7252–7267 (2018).
7. Z. Liu, J. Liu, Y. Zeng, and J. Ma, "Covert wireless communications in IOT systems: hiding information in interference," IEEE Wireless Commun. **25**, 46–52 (2018).
8. T. Fortier and E. Baumann, "20 years of developments in optical frequency comb technology and applications," Commun. Phys. **2**, 153 (2019).
9. S. A. Diddams, K. Vahala, and T. Udem, "Optical frequency combs: coherently uniting the electromagnetic spectrum," Science **369**, eaay3676 (2020).
10. M. Giunta, M. Fischer, W. Hänsel, T. Steinmetz, M. Lessing, S. Holzberger, C. Cleff, T. W. Hänsch, M. Mei, and R. Holzwarth, "20 years and 20 decimal digits: a journey with optical frequency combs," IEEE Photon. Technol. Lett. **31**, 1898–1901 (2019).
11. T. Herr, V. Brasch, J. D. Jost, C. Y. Wang, N. M. Kondratiev, M. L. Gorodetsky, and T. J. Kippenberg, "Temporal solitons in optical microresonators," Nat. Photonics **8**, 145–152 (2014).
12. V. Brasch, M. Geiselmann, T. Herr, G. Lihachev, M. H. Pfeiffer, M. L. Gorodetsky, and T. J. Kippenberg, "Photonic chip–based optical frequency comb using soliton Cherenkov radiation," Science **351**, 357–360 (2016).
13. A. Parriaux, K. Hammani, and G. Millot, "Electro-optic frequency combs," Adv. Opt. Photon. **12**, 223–287 (2020).
14. M. Zhang, B. Buscaino, C. Wang, A. Shams-Ansari, C. Reimer, R. Zhu, J. M. Kahn, and M. Lončar, "Broadband electro-optic frequency comb generation in a lithium niobate microring resonator," Nature **568**, 373–377 (2019).
15. A. Rueda, F. Sedlmeir, M. Kumari, G. Leuchs, and H. G. Schwefel, "Resonant electro-optic frequency comb," Nature **568**, 378–381 (2019).
16. J. Ma, X. Jiang, and M. Xiao, "Kerr frequency combs in large-size, ultra-high-*Q* toroid microcavities with low repetition rates [invited]," Photon. Res. **5**, B54–B58 (2017).
17. X. Yan, X. Zou, W. Pan, L. Yan, and J. Azaña, "Fully digital programmable optical frequency comb generation and application," Opt. lett. **43**, 283–286 (2018).
18. A. L. Gaeta, M. Lipson, and T. J. Kippenberg, "Photonic-chip-based frequency combs," Nat. Photonics **13**, 158–169 (2019).
19. C. Qin, K. Jia, Q. Li, T. Tan, X. Wang, Y. Guo, S.-W. Huang, Y. Liu, S. Zhu, Z. Xie, Y. Rao, and Y. Baicheng, "Electrically controllable laser frequency combs in graphene-fibre microresonators," Light Sci. Appl. **9**, 185 (2020).

20. J. Pan, B. Zhang, Z. Liu, J. Zhao, Y. Feng, L. Wan, and Z. Li, "Microbubble resonators combined with a digital optical frequency comb for high-precision air-coupled ultrasound detectors," Photon. Res. **8**, 303–310 (2020).
21. X. Wei, Y. Shen, J. C. Jing, A. S. Hemphill, C. Yang, S. Xu, Z. Yang, and L. V. Wang, "Real-time frequency-encoded spatiotemporal focusing through scattering media using a programmable 2D ultrafine optical frequency comb," Sci. Adv. **6**, eaay1192 (2020).
22. N. Picqué and T. W. Hänsch, "Frequency comb spectroscopy," Nat. Photonics **13**, 146–157 (2019).
23. Y. Bao, X. Yi, Z. Li, Q. Chen, J. Li, X. Fan, and X. Zhang, "A digitally generated ultrafine optical frequency comb for spectral measurements with 0.01-pm resolution and 0.7-μs response time," Light Sci. Appl. **4**, e300 (2015).
24. V. Torres-Company and A. M. Weiner, "Optical frequency comb technology for ultra-broadband radio-frequency photonics," Laser Photon. Rev. **8**, 368–393 (2014).
25. P. Marin-Palomo, J. N. Kemal, M. Karpov, A. Kordts, J. Pfeifle, M. H. Pfeiffer, P. Trocha, S. Wolf, V. Brasch, M. H. Anderson, R. Rosenberger, K. Vijayan, W. Freude, T. J. Kippenberg, and C. Koos, "Microresonator-based solitons for massively parallel coherent optical communications," Nature **546**, 274–279 (2017).
26. X. Xu, J. Wu, T. G. Nguyen, M. Shoeiby, S. T. Chu, B. E. Little, R. Morandotti, A. Mitchell, and D. J. Moss, "Advanced RF and microwave functions based on an integrated optical frequency comb source," Opt. Express **26**, 2569–2583 (2018).
27. R. N. McDonough and A. D. Whalen, *Detection of Signals in Noise*, 2nd ed. (Academic, 1995).
28. V. Ataie, D. Esman, B. P.-P. Kuo, N. Alic, and S. Radic, "Subnoise detection of a fast random event," Science **350**, 1343–1346 (2015).
29. D. Esman, V. Ataie, B. P.-P. Kuo, N. Alic, and S. Radic, "Subnoise signal detection and communication," J. Lightwave Technol. **34**, 5214–5219 (2016).
30. B. Crockett, L. R. Cortés, S. R. Konatham, and J. Azaña, "Single-shot subnoise signal recovery by coherent spectral energy redistribution," in *CLEO: Applications and Technology* (Optical Society of America, 2019), paper JW2A-71.
31. G. Agrawal, *Nonlinear Fiber Optics*, 5th ed. (Academic, 2012).
32. R. M. Wood, *Laser Damage in Optical Materials* (Adam Hilger, 1986).
33. B. C. Stuart, M. D. Feit, S. M. Herman, A. M. Rubenchik, B. W. Shore, and M. D. Perry, "Ultrashort-pulse optical damage," Proc. SPIE **2714**, 616–629 (1996).